Lattice Explorations of TeV Physics

Thomas Appelquist

Department of Physics, Sloane Laboratory, Yale University, New Haven, Connecticut, 06520, USA

I discuss the extent of the conformal window for an $SU(3)$ gauge theory with N_f Dirac fermions in the fundamental representation. I describe some recent work concluding that the theory is conformal in the infrared for $N_f = 12$, governed by an infrared fixed point, whereas the $N_f = 8$ theory exhibits confinement and chiral symmetry breaking. Thus the low end of the conformal window N_f^c lies in the range $8 \leq N_f^c \leq 12$. I discuss open questions and the potential relevance to physics beyond the standard model.

§1. Introduction

The conformal window in a gauge field theory with N_f light fermions is the range of N_f values such that the theory is asymptotically free and the infrared coupling is governed by an infrared fixed point. In an $SU(N)$ gauge theory with N_f Dirac fermions in the fundamental representation, the conformal window extends from $11N/2$ down to some critical value N_f^c at which a transition is expected to a phase in which chiral symmetry is broken spontaneously, and confinement sets in. In two recent papers,[1),2)] Fleming, Neil, and I provided nonperturbative evidence, using lattice simulations, that the lower end of the conformal window for the $SU(3)$ gauge theory lies in the range $8 < N_f^c < 12$.

Gauge theories in or near the conformal window could play a key role in describing physics beyond the standard model. If the fermions carry electroweak quantum numbers, and if N_f lies outside but near the conformal window, then the theory could drive electroweak breaking, forming the basis of walking technicolor theories. If the fermions do not carry electroweak quantum numbers, then N_f could lie within the conformal window, and the theory could describe some new, conformal sector, possibly coupled to the standard model through $SU(N)$ invariant operators.

To obtain the result $8 < N_f^c < 12$ for Dirac fermions in the fundamental representation of an $SU(3)$ gauge group, we employed a gauge invariant, nonperturbative running coupling derived from the Schrödinger functional of the gauge theory.[3)–5)] Defined within a Euclidean box of volume $O(L^4)$, it avoids typical finite volume effects by using L itself as the sliding scale. For the asymptotically free theories being considered, it agrees with the perturbative running coupling coupling at small enough L, and can be used to probe for conformal behavior in the large L limit. We made use of staggered fermions as in Ref. 6), and therefore restricted attention to values of N_f that are multiples of 4. The value $N_f = 16$ leads to an infrared fixed point that is so weak that it is best studied in perturbation theory. The value $N_f = 4$ is expected to be well outside the conformal window, leading to confinement and chiral symmetry breaking[7)] as with $N_f = 2$. We thus focused on the two values $N_f = 8$ and $N_f = 12$. We argued that for $N_f = 12$, the theory is indeed conformal in the infrared. For $N_f = 8$, we showed that the theory breaks chiral symmetry and confines. There is no evidence for an infrared fixed point.

§2. The conformal window

The existence of a conformal window in $SU(N)$ gauge theories has been known since the computation of the two-loop beta function by Caswell in 1974.[8] If the number of massless fermions N_f is near but just below the number N_f^{af} at which asymptotic freedom sets in, then the two-loop term is opposite in sign to the one-loop term and the resultant infrared fixed point is weak, accessible in perturbation theory. There is no confinement and chiral symmetry is unbroken. As N_f is reduced, the strength of the infrared fixed point grows, with N_f ultimately reaching the value N_f^{c} at which the transition to the chirally broken and confining phase is thought to set in. There is no a priori reason to expect the infrared fixed point to remain perturbative through this window.

If the theory is formulated in the continuum and a running coupling $\overline{g}^2(L)$ is defined at some length scale L, we have $L(\partial/\partial L)\overline{g}^2(L) = \overline{\beta}\left(\overline{g}^2(L)\right)$, where

$$\overline{\beta}\left(\overline{g}^2(L)\right) = b_1\overline{g}^4(L) + b_2\overline{g}^6(L) + b_3\overline{g}^8(L) + b_4\overline{g}^{10}(L) + \cdots \,. \qquad (2\cdot1)$$

For the case of $SU(3)$, the first two, universal coefficients are

$$b_1 = \tfrac{2}{(4\pi)^2}\left[11 - \tfrac{2}{3}N_f\right], \quad b_2 = \tfrac{2}{(4\pi)^4}\left[102 - \tfrac{38}{3}N_f\right]. \qquad (2\cdot2)$$

The next two coefficients depend on the renormalization scheme. In the $\overline{\mathrm{MS}}$ scheme, they are given by[9]

$$b_3^{\overline{\mathrm{MS}}} = \frac{2}{(4\pi)^6}\left[\frac{2857}{2} - \frac{5033}{18}N_f + \frac{325}{54}N_f^2\right], \qquad (2\cdot3)$$

and

$$b_4^{\overline{\mathrm{MS}}} = \frac{2}{(4\pi)^8}\left(29243.0 - 6946.30N_f + 405.089N_f^2 + 1.49931N_f^3\right). \qquad (2\cdot4)$$

For N_f close to $33/2$, the two-loop infrared fixed point value $\overline{g}_*^2$ is very small, and therefore corrected very little by the higher order terms.

For $N_f = 12$, there is a two-loop infrared fixed point at $\overline{g}_*^2 \simeq 9.48$, corrected to $\simeq 5.47$ at three loops in the $\overline{\mathrm{MS}}$ scheme, and to $\simeq 5.91$ at four loops. The convergence of the loop expansion is not guaranteed, but the fact that the expansion parameter at the fixed point $\overline{g}_*^2/4\pi$ is relatively small suggests that it could be reliable, and therefore that $N_f = 12$ lies inside the conformal window. For $N_f = 8$, there is no two-loop infrared fixed point. A fixed point can appear at three loops and beyond in some schemes, but its scheme dependence and typically large value means that there is no reliable evidence for an infrared fixed point accessible in perturbation theory. A nonperturbative study is essential.

§3. The Schrödinger functional

The Schrödinger functional is the partition function describing the quantum mechanical evolution of a system from a prescribed state at time $t = 0$ to another state at time $t = T$ in a spatial box of size L with periodic boundary conditions.[3)–5)] Dirichlet boundary conditions are imposed at $t = 0$ and $t = T$ where T is $O(L)$. They are chosen such that the minimum-action configuration is a constant chromo-electric background field of strength $O(1/L)$. This can be implemented in the continuum[3)] or with lattice regularization.[10)]

The Schrödinger functional can be represented as the path integral

$$\mathcal{Z}[W,\zeta,\overline{\zeta};W',\zeta',\overline{\zeta}'] = \int [DAD\psi D\overline{\psi}]e^{-S_G(W,W')-S_F(W,W',\zeta,\overline{\zeta},\zeta',\overline{\zeta}')}, \tag{3·1}$$

where A is the gauge field and ψ, $\overline{\psi}$ are the fermion fields. W and W' are the boundary values of the gauge fields, and $\zeta,\overline{\zeta},\zeta',\overline{\zeta}'$ are the boundary values of the fermion fields at $t = 0$ and $t = T$, respectively.

Although the Schrödinger functional can be formulated completely in the continuum, from here on I will introduce a Euclidean spacetime lattice. The quantity S_G is chosen to be the standard Wilson gauge action[11)] with a boundary improvement counterterm. For the fermionic action, we made use of the staggered approach as in Ref. 6), which reduces the 16 doubler species of a naively discretized fermion field to 4 degrees of freedom. In the continuum limit, a single staggered fermion field can be interpreted as four degenerate Dirac fermion fields.

The gauge boundary values W, W' were chosen such that the minimum-action configuration is a constant chromoelectric field whose magnitude is of $O(1/L)$ and is controlled by a dimensionless parameter η.[12)] The Schrödinger functional (SF) running coupling is then defined in terms of the response of the action to variations in η:

$$\frac{k}{\overline{g}^2(L,T)} = -\frac{\partial}{\partial\eta}\log\mathcal{Z}\bigg|_{\eta=0}, \tag{3·2}$$

where

$$k = 12\left(\frac{L}{a}\right)^2\left[\sin\left(\frac{2\pi a^2}{3LT}\right)+\sin\left(\frac{\pi a^2}{3LT}\right)\right]. \tag{3·3}$$

The factor k is chosen so that $\overline{g}^2(L,T)$ equals the bare coupling at tree level. In general, $\overline{g}^2(L,T)$ measures the response of the system to small changes in the background chromo-electric field.

The fermionic Dirichlet boundary values $\zeta,\overline{\zeta},\zeta',\overline{\zeta}'$ are subject only to multiplicative renormalization for staggered fermions.[13)] We took them equal to zero, simplifying the calculation.

The staggered approach to discretization of fermions can be thought of as splitting the 16 degrees of freedom of a single spinor over a 2^4 hypercube of lattice sites. This framework requires an even number of lattice sites in each direction. Thus with periodic boundary conditions in space, the spatial extent L/a of the lattice must be even. However, in the Schrödinger functional formalism, the Dirichlet boundaries in the time direction require an odd temporal extent T/a in order for the number of lattice sites to be even, since the sites located at $t=0$ and $t=T$ are distinct.

As a result, one can simulate only with $T = L \pm a$. In the continuum limit $T=L$ is recovered, but at a finite lattice spacing this results in the introduction of $O(a)$ lattice artifacts into observables. This is undesirable, since staggered fermion simulations contain bulk artifacts only at $O(a^2)$ and higher. Fortunately, simulating at $T = L \pm a$ and averaging over the observed values eliminates this effect.[6] We adopted this technique, defining the central observable

$$\frac{1}{\overline{g}^2(L)} = \frac{1}{2}\left[\frac{1}{\overline{g}^2(L, L-a)} + \frac{1}{\overline{g}^2(L, L+a)}\right], \tag{3·4}$$

which depends on only one large distance scale L. To be more explicit, this running coupling can be written as $\overline{g}^2(\beta, L/a)$ where $\beta \equiv 2N/g_0^2$. From this point on I will fix $N=3$, and so $\beta = 6/g_0^2$.

The SF coupling $\overline{g}^2(L)$ has been normalized to give the bare lattice coupling g_0^2 at tree level. With the lattice as a regulator, it can be expanded as a power series in g_0^2 with coefficients depending on a/L. By rearranging this series in terms of a coupling defined at an arbitrary scale and setting to zero terms that vanish as $a \to 0$, a continuum beta function can be defined. Its perturbation expansion leads to the universal coefficients b_1 and b_2 of Eq. (2·2) at the one- and two-loop levels. The three-loop, scheme-dependent coefficient has been computed in this Schrödinger functional scheme by combining the two-loop perturbative computation of the SF running coupling in lattice perturbation theory with a similar lattice computation of the $\overline{\mathrm{MS}}$ coupling constant.[10] The result is

$$b_3^{\mathrm{SF}} = b_3^{\overline{\mathrm{MS}}} + \frac{b_2 c_2}{4\pi} - \frac{b_1(c_3 - c_2^2)}{16\pi^2}, \tag{3·5}$$

where $b_3^{\overline{\mathrm{MS}}}$ is given by Eq. (2·3) with $c_2 = 1.256 + 0.040 N_f$ and $c_3 = c_2^2 + 1.197(10) + 0.140(6)N_f - 0.0330(2)N_f^2$. The perturbative behavior based on the $\overline{\mathrm{MS}}$ scheme, is qualitatively unchanged by the modification of the three-loop coefficient. For $N_f = 12$, the three-loop SF coupling has a fixed point at $\overline{g}_\star^2 \approx 5.18$, compared with $\overline{g}_\star^2 \approx 5.47$ at three loops in the $\overline{\mathrm{MS}}$ scheme.

The four-loop coefficient in the SF scheme has not yet been computed. But the fact that in the $\overline{\mathrm{MS}}$ scheme the four-loop correction shifts the fixed point by less than 10% from its three-loop value suggests that the same may be true in the SF scheme. This indicates that perturbation theory could be reliable to describe infrared behavior for $N_f = 12$, and that the infrared fixed point might truly exist. For $N_f = 8$, since the universal one- and two-loop coefficients are both positive, there is no reliable, perturbative evidence for the existence of an infrared fixed point. As already noted, a nonperturbative study is essential.

§4. Lattice simulations

To measure the running coupling on the lattice, we generated an ensemble of gauge configurations distributed with the appropriate weighting by the Euclidean action. The running coupling was then computed as an average over this ensemble. Simulations were performed using the MILC code,[14] with some customization. Evolution of the gauge configurations was accomplished using the hybrid molecular dynamics (HMD) approach, with the fermionic contribution included using the R algorithm.[15]

Sets of gauge configurations were generated at each box size L/a and bare coupling β. Two independent ensembles were created at $T/a = L/a \pm 1$, and then averaged together as in Eq. (3·4). The data were collected over a wide range of β values and for $6 \leq L/a \leq 20$, in order to capture the evolution of $\overline{g}^2(L)$ over a large range of scales. In the range of β values employed, for both $N_f = 8$ and $N_f = 12$, there is no evidence for a bulk phase transition. We explored this issue by examining the plaquette time series within this range and at lower values of β. At lower values, we indeed found evidence for a bulk phase transition. These lower values are, however, well separated from the minimum β used in our analysis.

The goal is to map out the behavior of the running coupling over a large range of scales L. However, the range over which one can measure the coupling strength with fixed lattice spacing a before the computational expense becomes prohibitive is still rather limited. To achieve our goal, we used a procedure known as step scaling.[16],[17]

Step scaling provides a systematic way to combine multiple lattice measurements of the running coupling $\overline{g}^2(L)$ into a single measurement of the continuum evolution of the coupling as the scale changes from $L \to sL$, where s is a scaling factor called the step size. In a continuum setting, the evolution is described by the "step-scaling function",

$$\sigma(s, \overline{g}^2(L)) \equiv \overline{g}^2(sL), \tag{4·1}$$

which can be thought of as a discrete version of the usual continuum evolution described by the beta function. In a lattice calculation, the extracted step-scaling function will be a function also of a/L, which we must extrapolate to the continuum:

$$\sigma(s, \overline{g}^2(L)) = \lim_{a \to 0} \Sigma(s, \overline{g}^2(L), a/L). \tag{4·2}$$

Step scaling is generically implemented by first choosing an initial value $u = \overline{g}^2(L)$. Several ensembles with different values of a/L are then generated, with β tuned so that the coupling measured on each is equal to the chosen value, $\overline{g}^2(L) = u$. A second ensemble is generated at each β, but with $L \to sL$. The value of the coupling measured on this larger lattice is exactly $\Sigma(s, u, a/L)$. An extrapolation $a/L \to 0$ can then recover the continuum value $\sigma(s, u)$. Taking $\sigma(s, u)$ to be the new starting value, one can then iterate this procedure until we have sampled $\overline{g}^2(L)$ over a large range of L values. In practice we took $s = 2$.

There is a natural caveat on the step-scaling procedure. In the limit $a/L \to 0$ with $\overline{g}^2(L)$ fixed, $g_0^2(a/L)$ depends on the short-distance behavior of the theory, and it is important that it remains bounded so that it does not trigger a bulk phase transition. If asymptotic freedom governs the short distance behavior, this is automatic since $g_0^2(a/L) \to 1/\log(L/a)$. While this is our principal focus, the existence of an infrared fixed point for the $N_f = 12$ theory will lead us to consider also values of $\overline{g}^2(L)$ lying above the fixed point. Then $g_0^2(a/L)$ increases as $a \to 0$, with no evidence from our simulations that it remains bounded and therefore that the continuum limit exists. Nevertheless, one can consider small values of a/L providing that $g_0^2(a/L)$ remains small enough not to trigger a bulk phase transition.

Carrying out the above procedure directly can be expensive in computational power since each tuning of β may require several attempts. We instead measured $\overline{g}^2(L)$ for a limited set of values for β and L/a, and then generated an interpolating function. This function was used to tune β as described above. In Ref. 2), we employed a set of interpolating functions, one for each L/a, focused on the lattice observable $1/\overline{g}^2(\beta, L/a)$. We used a fit at each L/a with n-th order polynomial dependence on $g_0^2 = 6/\beta$:

$$\frac{1}{\overline{g}^2(\beta, L/a)} = \frac{\beta}{6}\left[1 - \sum_{i=1}^{n} c_{i,L/a}\left(\frac{6}{\beta}\right)^i\right]. \tag{4·3}$$

The order n of the polynomial was varied with L/a in order to achieve the optimal χ^2 per degree of freedom when fitting to the data. The values of the parameters with associated errors, determined by fits to the simulation data for both $N_f = 8$ and $N_f = 12$, are discussed in Ref. 2).

This function is used for interpolation within the measured range, as a basis for the step-scaling procedure. More elaborate interpolating functions could be used, in particular, modeling explicitly the L/a dependence or including nonanalytic terms in g_0^2, but such functional forms do not significantly alter the fit quality or the results of step scaling based on the collected data set.

We accounted for numerous sources of statistical and systematic error.[2)] We concluded that potential systematic errors in our procedure are small compared to current statistical errors.

§5. Results

5.1. $N_f = 8$

The simulation data for $\overline{g}^2(L)$ as a function of β and L/a are displayed in Ref. 2). The ranges are $\beta = 4.55$–192 and $L/a = 6, 8, 10, 12, 16$. The lower limit on β was chosen to insure that the lattice coupling is weak enough so as not to induce a bulk phase transition. The upper limit was taken to be large so that we could check the agreement of our simulations with perturbation theory when the coupling is very weak. The final results depend sensitively only on simulations below $\beta = 10$. The data becomes more sparse with increasing L/a, reflecting the growing computational time involved. In particular, only a very limited amount of $L/a = 20$ data, at very weak coupling, is available at $N_f = 8$, so we excluded these points from our analysis. The $L/a = 10$ data is thus also excluded, since it cannot be used in step scaling at $s = 2$ without the $L/a = 20$ points. The resultant values of $\overline{g}^2(L)$ are perturbative ($\overline{g}^2(L)/4\pi \ll 1$) throughout much of the range, except for small β.

In order to carry out the step-scaling procedure, we employed the interpolating function of Eq. (4·3). The resulting best-fit mean values and errors for the parameters at each L/a are discussed in Ref. 2). In Fig. 1, data points are shown together with

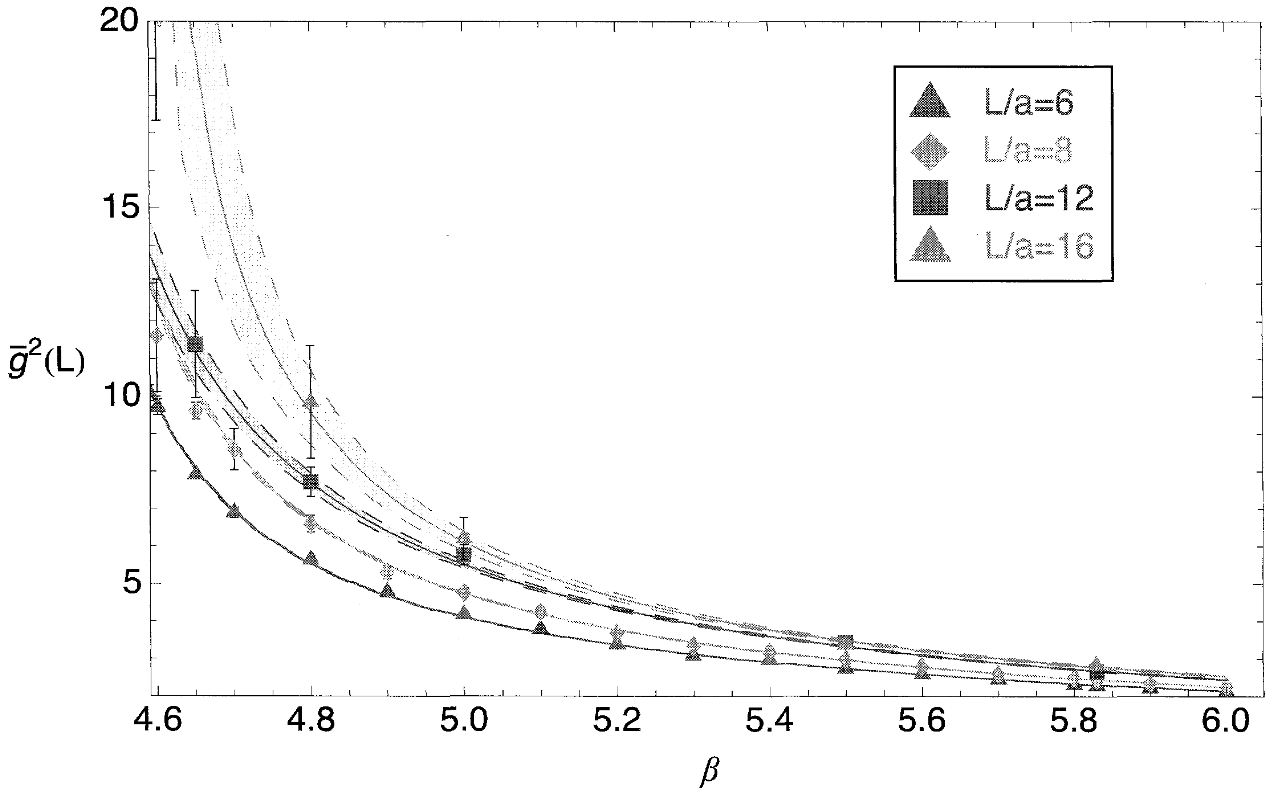

Fig. 1. (color online) Measured values $\overline{g}^2(L)$ versus β for $N_f = 8$. The interpolating curves shown represent the best fit to the data, using the functional form Eq. (4·3). The errors are statistical.

the interpolating functions for $\overline{g}^2(L)$ as a function of β, for each of $L/a = 6, 8, 12, 16$.

Figure 2 shows a typical continuum extrapolation from our 8-flavor data. The points shown represent steps from $L/a = 6 \to 12$ and $8 \to 16$. Constant extrapolation (a weighted average of the two points) is used since the lattice-artifact contributions to $\Sigma(2, u, a/L)$ are small compared to the statistical errors. We estimated the systematic error in this procedure and found that it is small compared to the statistical error.

Our results for the continuum running of $\overline{g}^2(L)$ are shown in Fig. 3. L_0 is the scale at which $\overline{g}^2(L_0) = 1.6$, a relatively weak value. The points are shown for values of L/L_0 increasing by factors of 2. The (statistical) errors are derived as described in Ref. 2). For comparison, the perturbative running of $\overline{g}^2(L)$ at two loops and three loops is shown up through $\overline{g}^2(L) \approx 10$ where perturbation theory is no longer expected to be accurate. The results show that the coupling evolves according to perturbation theory up through $\overline{g}^2(L) \approx 4$, and then increases more rapidly, reaching values that clearly exceed typical estimates of the strength required to trigger spontaneous chiral symmetry breaking.[18] The dynamical fermion mass is of order of the corresponding $1/L$, and since the coupling is strong here, the theory will confine at roughly this distance scale. There is no evidence for an infrared fixed point or even an inflection point in the behavior of $\overline{g}^2(L)$.

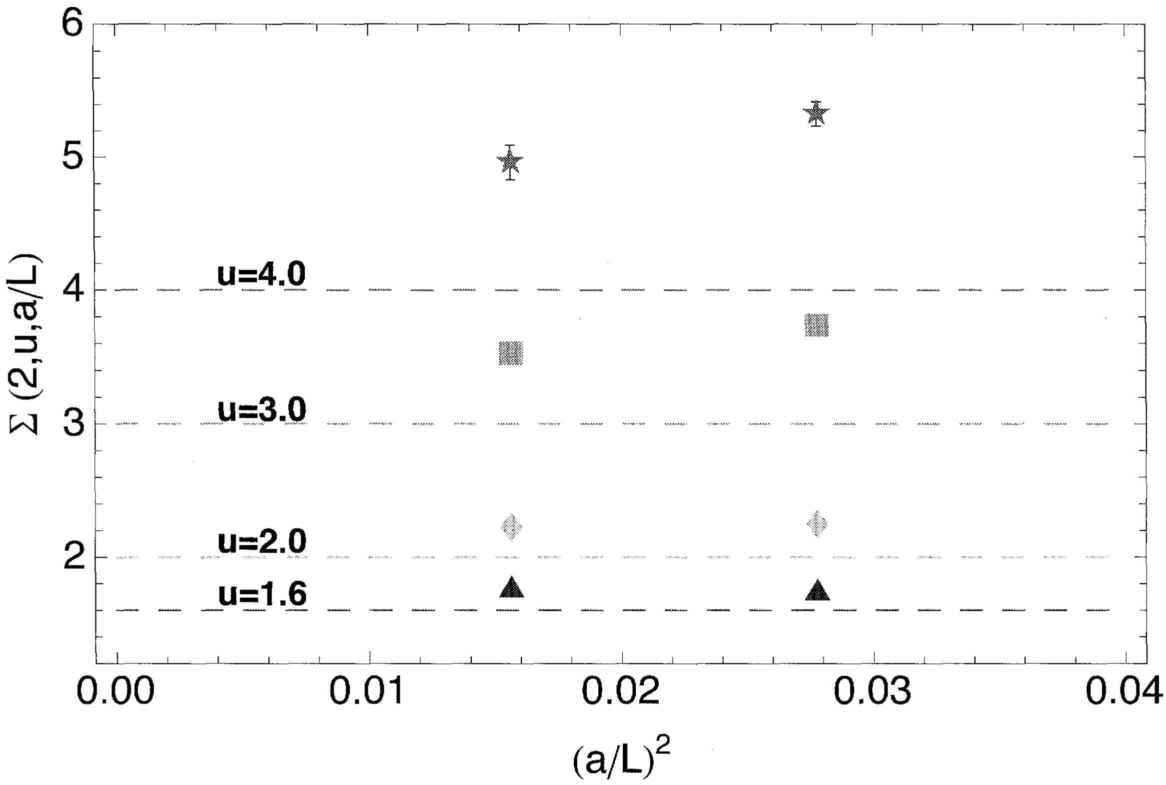

Fig. 2. (color online) Step-scaling function $\Sigma(2, u, a/L)$ at various u, for each of the two steps $L/a = 6 \to 12$ and $8 \to 16$ used in the $N_f = 8$ analysis. Note that $\Sigma(2, u, a/L) > u$ in each case, with the difference increasing as u increases.

5.2. $N_f = 12$

The simulation data for $\overline{g}^2(L)$ as a function of β and L/a are also displayed in Ref. 2). The table ranges from $\beta = 4.2$–192 and $L/a = 6$–20. The lower limit on β insures that the lattice coupling is weak enough so as not to induce a bulk phase transition. As in the $N_f = 8$ case, the upper limit was taken to be large in order to explore agreement with perturbation theory, but data above $\beta = 10$ do not have significant influence on our analysis. $L/a = 20$ data were included here and not in the $N_f = 8$ case because of concerns about the magnitude of the lattice artifact corrections, compared to the continuum running. In the end, artifact corrections were found to be small compared to our statistical error. The interpolating functional form Eq. (4·3) was again employed, and the resulting best-fit mean values and errors of the parameters at each L/a are discussed in Ref. 2). In Fig. 4, data points are shown for $\overline{g}^2(L)$ as a function of β, together with the interpolating functions for each of $L/a = 6, 8, 10, 12, 16, 20$.

The data and the interpolating curves already suggest the existence of an infrared fixed point for $N_f = 12$. For small β, the general trend is that $\overline{g}^2(L)$ decreases with increasing L. This behavior and the fact that for larger β, $\overline{g}^2(L)$ increases with increasing L, are reflected in a crossover behavior in the interpolating curves. We first implemented the step-scaling procedure choosing an initial $u = \overline{g}^2(L)$ well below a possible fixed-point value so that a continuum limit is guaranteed to exist. A constant continuum extrapolation (a weighted average of the available values of

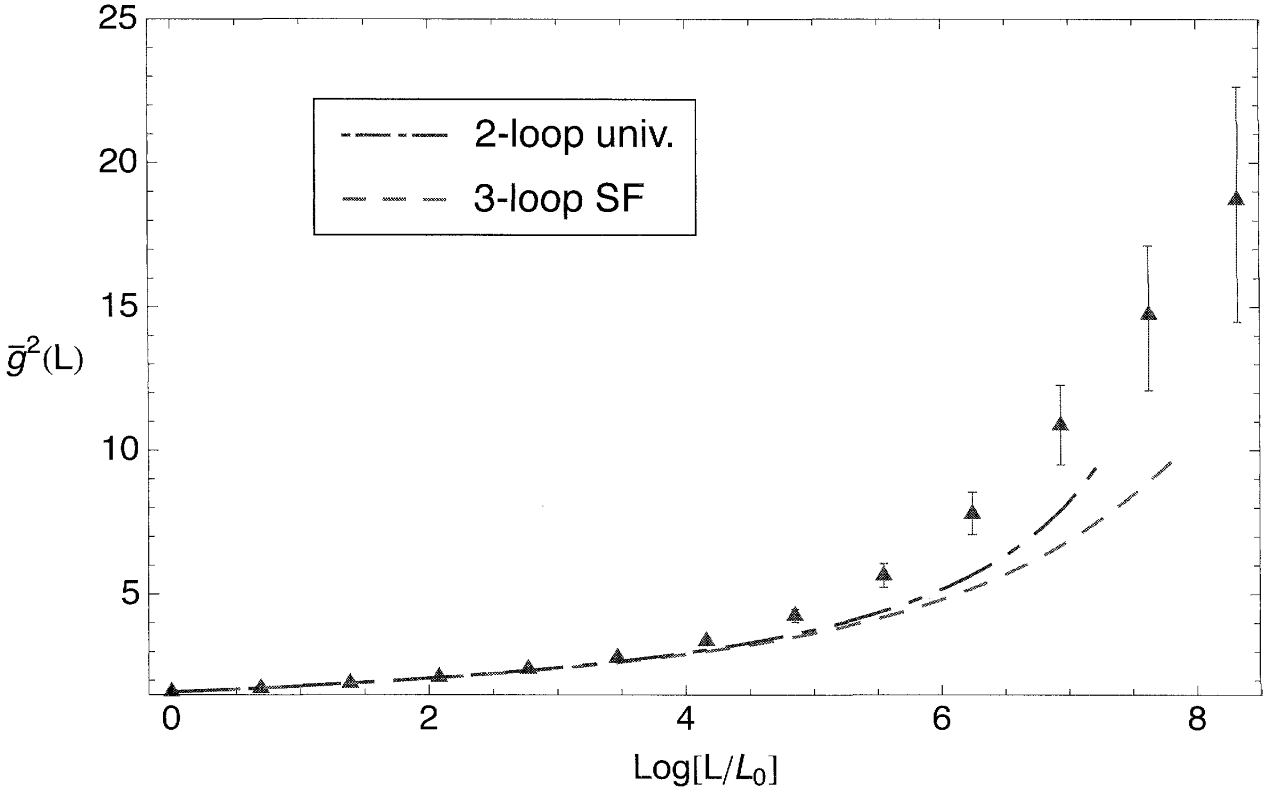

Fig. 3. (color online) Continuum running for $N_f = 8$. Purple points are derived by step-scaling using the constant continuum-extrapolation of Fig. 2. The error bars shown are purely statistical. Two-loop and three-loop perturbation theory curves are shown for comparison.

$\Sigma(2, u, a/L))$ was again employed for each u. Now, since we have data at $L = 20$, the extrapolation is a weighted average of three points corresponding to the steps $6 \to 12$, $8 \to 16$, and $10 \to 20$. Examples of such a continuum extrapolation are shown in Fig. 5. The systematic error is again estimated to be small compared to the statistical error.

Our results for the continuum running of $\bar{g}^2(L)$ from small values are shown in purple in Fig. 6. L_0 is again taken to be the scale at which $\bar{g}^2(L_0) = 1.6$. The points are shown for for values of L/L_0 increasing by factors of 2. The (statistical) errors are derived as described in Ref. 2). For reference, the two-loop and three-loop perturbative curves for $\bar{g}^2(L)$ are also shown in Fig. 6. From the figure, we conclude that the infrared behavior is indeed governed by a fixed point whose value lies within the statistical error band. Because of the underlying use of an interpolating function, the error bars of adjacent points in Fig. 6 are highly correlated. As the running coupling approaches the infrared fixed point, this correlation approaches 100%, so that the error bars asymptotically approach a stable value as the number of steps is taken to infinity. The range of possible values of the fixed point from our simulations is consistent with the three-loop perturbative value in the SF scheme, well below estimates[18)] of the strength required to trigger spontaneous chiral symmetry breaking and confinement.

The infrared fixed point also governs the $L \to \infty$ behavior starting from values

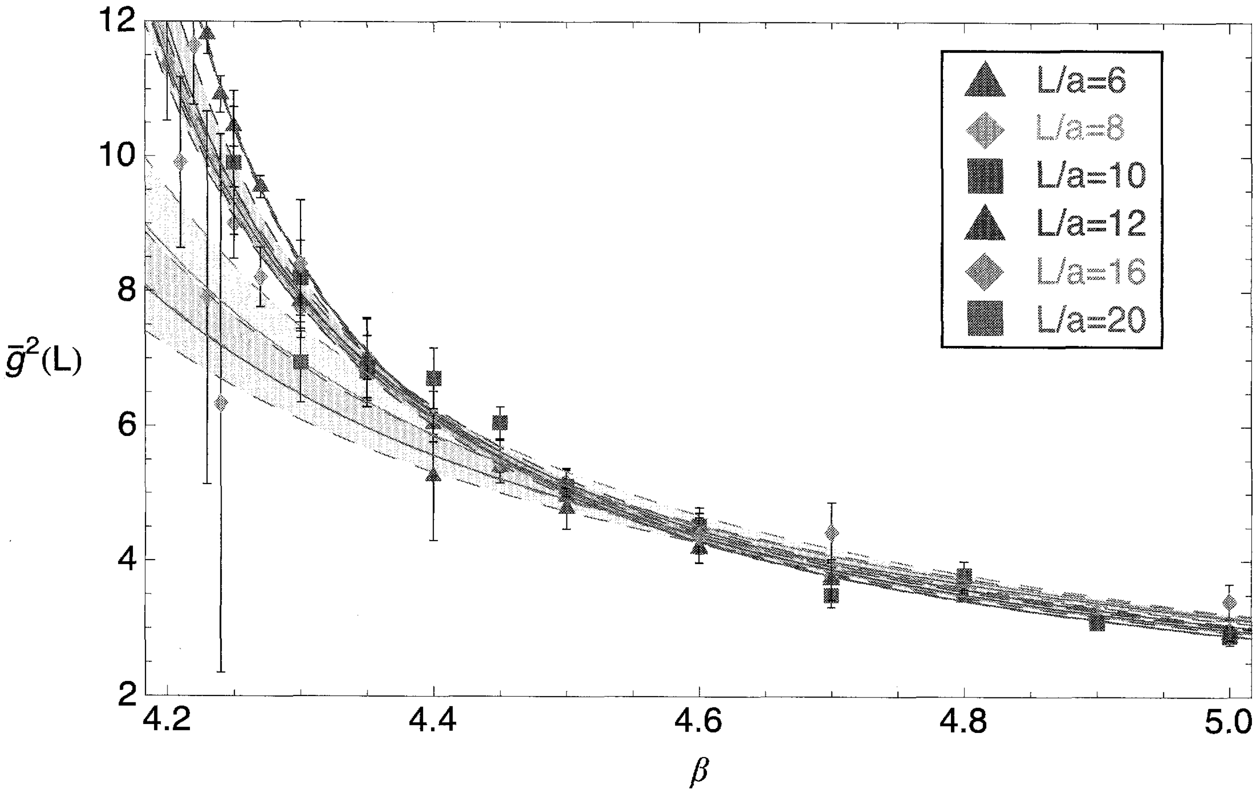

Fig. 4. (color online) Measured values $\bar{g}^2(L)$ versus β, $N_f = 12$. The interpolating curves shown represent the best fit to the data, using the functional form of Eq. (4·3).

of $\bar{g}^2(L)$ above the fixed point. As discussed already, the continuum limit is then no longer guaranteed to exist and the step-scaling procedure cannot be naively applied. Instead, one can restrict the discussion to finite but small values of a/L, small enough to minimize lattice artifacts but large enough so that for $\bar{g}^2(L)$ near but above the fixed point, $g_0^2(a/L)$ is small enough not to trigger a bulk phase transition. The step-scaling procedure then leads to the continuum running from above to the fixed point, also shown in Fig. 6. The statistical-error band is derived as in the approach from below.

§6. Summary

For an $SU(3)$ gauge theory with N_f Dirac fermions in the fundamental representation, the value $N_f = 8$ lies outside the conformal window, leading to confinement and chiral symmetry breaking, while $N_f = 12$ lies within the conformal window, governed by an infrared fixed point. The fixed point value is bounded as shown in Fig. 6. This is, as far as I know, the first nonperturbative evidence for the existence of infrared conformal behavior in a nonsupersymmetric gauge theory.

The $N_f = 8$ and $N_f = 12$ results imply that the lower end of the conformal window, N_f^c, lies in the range $8 < N_f^c < 12$. This conclusion is reached employing the Schrödinger functional (SF) running coupling, $\bar{g}^2(L)$, defined *at the box boundary* L with a set of special boundary conditions. This coupling is a gauge invariant quantity, valid for any coupling strength and running in accordance with perturbation theory

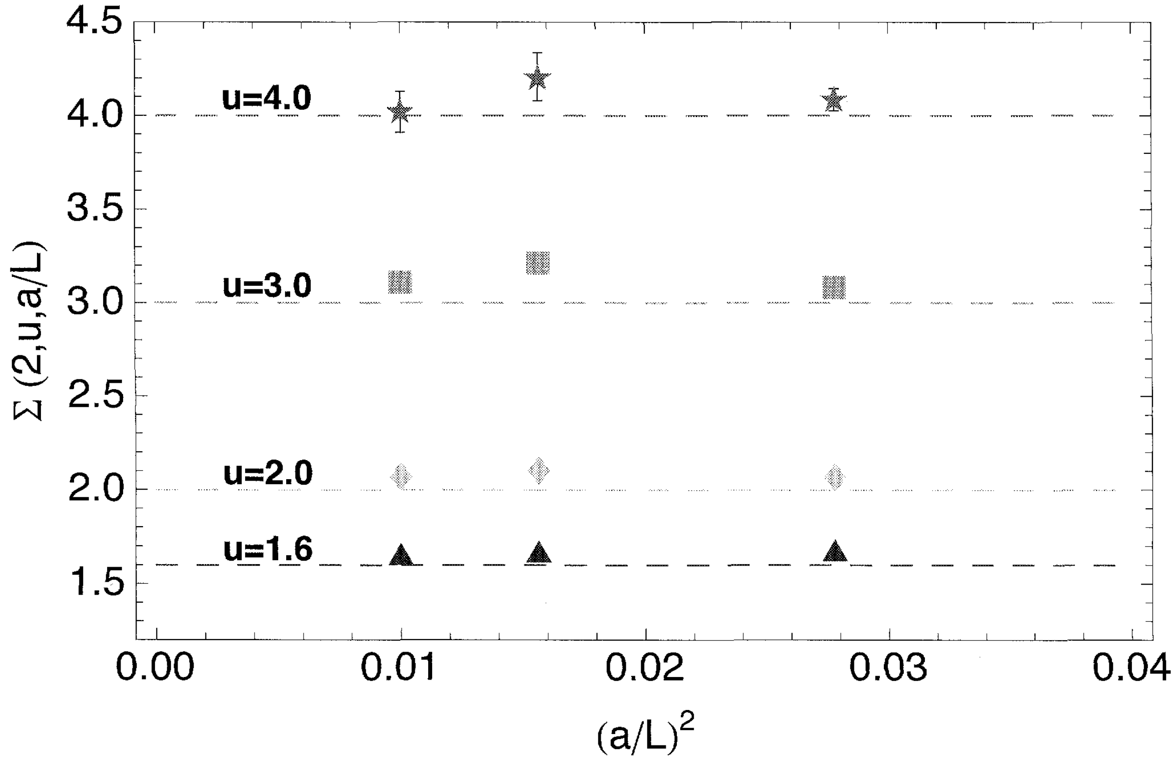

Fig. 5. (color online) Step-scaling function $\Sigma(2,u,a/L)$ at various u, for each of the three steps $L/a = 6 \to 12$, $8 \to 16$, $10 \to 20$ used in the $N_f = 12$ analysis. Note that $\Sigma(2,u,a/L) \to u$ as the starting coupling u approaches the fixed point value.

at short distances.

For $N_f = 8$, we simulated $\overline{g}^2(L)$ up through values that exceed typical estimates of the coupling strength required to trigger dynamical chiral symmetry breaking,[18] with no evidence for an infrared fixed point or even an inflection point. For $N_f = 12$, the observed infrared fixed point is rather weak, agreeing within the estimated errors with the three-loop fixed point in the SF scheme, and well below typical estimates of the coupling strength required to trigger dynamical chiral symmetry breaking.[18]

Whether perturbation theory can be used reliably to reproduce the behavior in the vicinity of the $N_f = 12$ fixed point remains to be seen. The three-loop value of the fixed point is substantially different from the two-loop value. On the other hand, in the $\overline{\text{MS}}$ scheme where the four-loop beta function has been computed, the four-loop fixed point is shifted by only a small amount from the three-loop value. The relative weakness of this fixed point, together with the fact that N_f^c cannot be much smaller, raises the question of whether the theory remains perturbative throughout the conformal window.[19]

It is important to confirm these results by employing other definitions of the running coupling, for example, based on the Wilson loop and static potential,[20] and by examining scheme-independent quantities. Most notably, spontaneously chiral symmetry breaking as a function of N_f should be studied through a zero-temperature lattice simulation of the chiral condensate. Simulations of $\overline{g}^2(L)$ for other values of N_f, in particular $N_f = 10$, are crucial to determine more accurately the lower end of the conformal window and to study the phase transition as a function of N_f. All

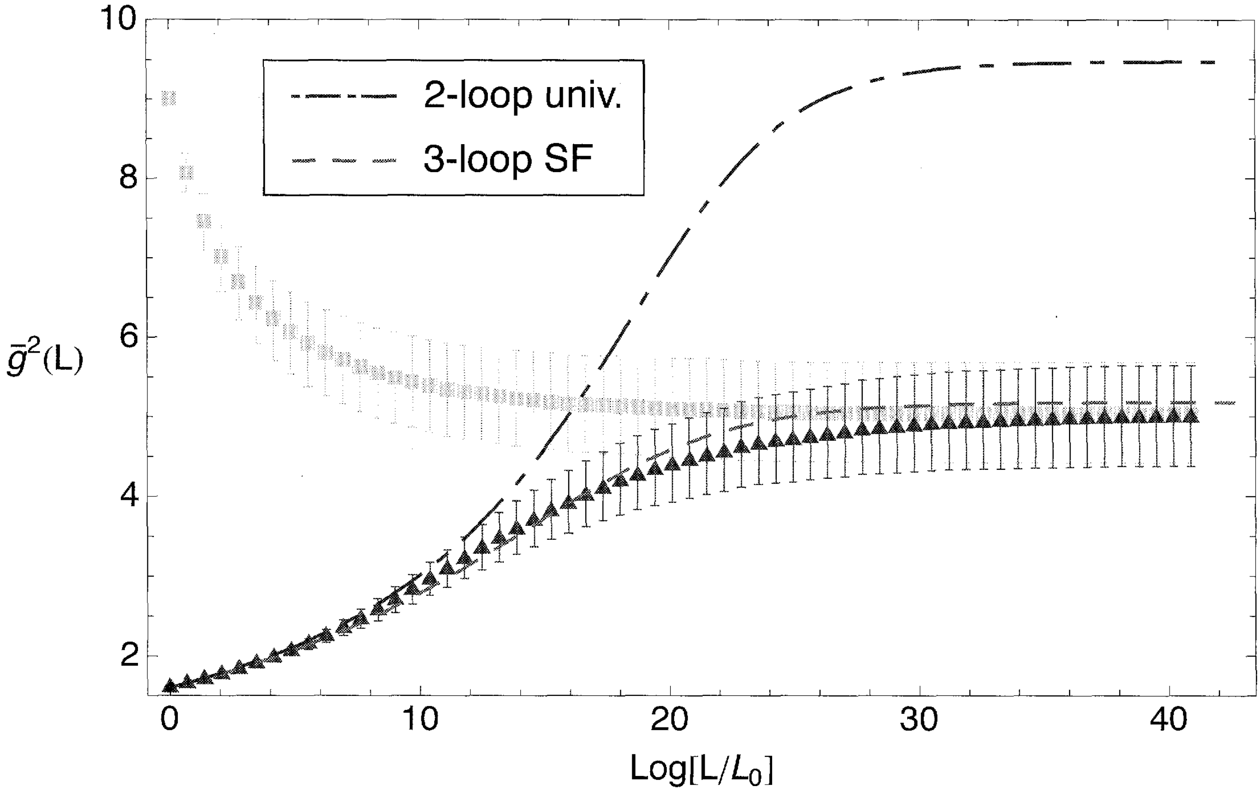

Fig. 6. (color online) Continuum running for $N_f = 12$. Results shown for running from below the infrared fixed point (purple triangles) are based on $\overline{g}^2(L_0) \equiv 1.6$. Also shown is continuum backwards running from above the fixed point (light blue squares), based on $\overline{g}^2(L_0) \equiv 9.0$. Error bars are again purely statistical, although strongly correlated due to the underlying interpolating functions. Two-loop and three-loop perturbation theory curves are shown for comparison.

of these analyses should be extended to other gauge groups and other representation assignments for the fermions.[21)–27)]

The phenomenological relevance of these studies remains to be seen. A theory with N_f outside but near the conformal window ($\lesssim N_f^c$) could describe electroweak breaking and provide the basis for walking technicolor.[28)] In this class of theories, as $N_f \to N_f^c$ from below, a hierarchy emerges between the electroweak scale and the larger mass scale where the gauge coupling becomes strong. This could be signaled by the appearance of a plateau of finite extent in $\overline{g}^2(L)$, and by the development of a hierarchy between the chiral condensate and the electroweak scale. It is also important to explore the particle spectrum in this limit and to compute the electroweak precision parameters, in particular the S parameter.

References

1) T. Appelquist, G. T. Fleming and E. T. Neil, Phys. Rev. Lett. **100** (2008), 171607, arXiv:0712.0609.
2) T. Appelquist, G. T. Fleming and E. T. Neil, Phys. Rev. D **79** (2009), 076010, arXiv:0901.3766.
3) M. Lüscher, R. Narayanan, P. Weisz and U. Wolff, Nucl. Phys. B **384** (1992), 168, hep-lat/9207009.

4) S. Sint, Nucl. Phys. B **421** (1994), 135, hep-lat/9312079.
5) A. Bode et al. (ALPHA Collaboration), Phys. Lett. B **515** (2001), 49, hep-lat/0105003.
6) U. M. Heller, Nucl. Phys. B **504** (1997), 435, hep-lat/9705012.
7) C. Z. Sui, Ph.D. thesis, Columbia University, New York, NY (2001), UMI-99-98219.
8) W. E. Caswell, Phys. Rev. Lett. **33** (1974), 244.
9) T. van Ritbergen, J. A. M. Vermaseren and S. A. Larin, Phys. Lett. B **400** (1997), 379, hep-ph/9701390.
10) A. Bode, P. Weisz and U. Wolff (ALPHA collaboration), Nucl. Phys. B **576** (2000), 517 [Errata; **600** (2001), 453], hep-lat/9911018.
11) K. G. Wilson, Phys. Rev. D **10** (1974), 2445.
12) M. Lüscher, R. Sommer, P. Weisz and U. Wolff, Nucl. Phys. B **413** (1994), 481, hep-lat/9309005.
13) R. Sommer, hep-lat/0611020.
14) C. DeTar et al. (MILC) (2002), `http://www.physics.utah.edu/~detar/milc/`
15) S. A. Gottlieb, W. Liu, D. Toussaint, R. L. Renken and R. L. Sugar, Phys. Rev. D **35** (1987), 2531.
16) M. Lüscher, P. Weisz and U. Wolff, Nucl. Phys. B **359** (1991), 221.
17) S. Caracciolo, R. G. Edwards, S. J. Ferreira, A. Pelissetto and A. D. Sokal, Phys. Rev. Lett. **74** (1995), 2969; hep-lat/9409004.
18) T. Appelquist, A. Ratnaweera, J. Terning and L. C. R. Wijewardhana, Phys. Rev. D **58** (1998), 105017, hep-ph/9806472.
19) E. Gardi and G. Grunberg, J. High Energy Phys. **03** (1999), 024, hep-th/9810192.
20) E. Bilgici et al., arXiv:0808.2875.
21) Y. Shamir, B. Svetitsky and T. DeGrand, Phys. Rev. D **78** (2008), 031502, arXiv:0803.1707.
22) S. Catterall, J. Giedt, F. Sannino and J. Schneible, J. High Energy Phys. **11** (2008), 009, arXiv:0807.0792.
23) L. Del Debbio, M. T. Frandsen, H. Panagopoulos and F. Sannino, J. High Energy Phys. **06** (2008), 007, arXiv:0802.0891.
24) A. J. Hietanen, J. Rantaharju, K. Rummukainen and K. Tuominen, J. High Energy Phys. **05** (2009), 025, arXiv:0812.1467.
25) L. Del Debbio, A. Patella and C. Pica, arXiv:0812.0570.
26) Z. Fodor, K. Holland, J. Kuti, D. Nogradi and C. Schroeder, arXiv:0809.4888.
27) L. Del Debbio, A. Patella and C. Pica, arXiv:0805.2058.
28) T. Appelquist and L. C. R. Wijewardhana, Phys. Rev. D **36** (1987), 568.